Pol. J. Environ. Stud. Vol. XX, No. X (XXXX), 1-14
DOI: *10.15244/pjoes/195374* ONLINE PUBLICATION DATE: 2025-01-15

Original Research

Low Impact Development Facility Layout in Landscape Design Based on the Coupling of NSGA-III Algorithm and BIM Technology

Ling Zhao[1, 2], Baijun Li[3]*

[1]School Design, Nanjing University of the Arts, Nanjing 210013, China
[2]School of Design and Innovation, Shenzhen University of Technology, Shenzhen 518118, Guangdong, China
[3]Foshan Overseas Chinese Town Real Estate Co., Ltd. Guangdong 528300, China

Received: 20 August 2024
Accepted: 28 October 2024

Abstract

Current low-impact development (LID) facility layout optimization methods focus too heavily on micro aspects, such as rainwater treatment, the applicability of technical measures, and the construction of individual LID facilities. This narrow focus neglects systemic issues across different scales and regions, resulting in suboptimal outcomes for LID facility layout optimization. Therefore, to improve the optimization of low-impact development facility layouts, different landscape features should be considered to minimize the impact of landscape construction on rainwater discharge and achieve sustainable landscape development. On this basis, a low-impact development facility layout optimization method using the Revit building information model and non-dominated sorting genetic algorithm-III was proposed. The experimental results show that the average peak signal-to-noise ratio of the Revit building information model is 0.057, and the average accuracy is 91.9%, making it more effective in extracting landscape features compared to other algorithms. In addition, after optimization, the reduction rates for biological reservoirs, grass ditches, and permeable pavement facilities were 78%, 59%, and 70%, respectively. Overall, the optimized low-impact development facilities account for 23.1% of the research area. This plan reduces the annual total runoff at the exit of the research area by 86.95%, effectively enhancing the overall performance of the low-impact development facility layout. The proposed layout optimization method, based on the Revit building information model and the non-dominated sorting genetic algorithm-III, optimizes the layout of low-impact development facilities according to landscape characteristics. Additionally, this method effectively reduces construction costs and rainwater runoff.

Keywords: landscape design, low impact development, revit BIM, NSGA-III, layout optimization

*e-mail: Baijun.BL_Li@outlook.com

Introduction

Low Impact Development (LID) is a rainstorm management and non-point source pollution treatment technology developed in the late 1990s. LID aims to control the runoff and pollution caused by rainstorms through decentralized and small-scale source control, so as to make the development area as close to the natural hydrological cycle as possible. LID facilities mainly include ecological grass ditches, sunken green spaces, rain gardens, green roofs, underground seepage storage, and permeable pavements [1-3]. LID highlights that urban development should downgrade its influence on the environment. The core principle is to establish an urban drainage system compatible with nature, based on the concepts of source control and delaying impact loads. Meanwhile, reasonable use of landscape space and corresponding measures are taken to control rainstorm runoff and reduce urban non-point source pollution [4, 5]. However, when carrying out landscape construction, this demand is often overlooked. This leads to unreasonable planning of LID facilities in the landscape area, resulting in the inability to discharge rainwater in a timely manner and an increase in runoff pollution. Meanwhile, due to the different characteristics of each landscape, it is difficult to achieve targeted LID facility layout planning. Therefore, it is necessary to develop an LID facility layout optimization (LO) model suitable for landscape design, which can accurately identify landscape characteristics and optimize LID facility layouts accordingly.

There have been numerous research findings on landscape feature extraction and recognition. Q. Zhang et al. proposed a feature analysis method using feature extraction and fused attention pyramid decoding for landscape feature analysis. This model adopted multi-scale feature extraction and fusion to capture landscape features at different levels and scales. Attention pyramid decoding was used to mine spatial and semantic information, thereby improving classification accuracy. This model outperformed other methods when applied to remote sensing images of traditional village landscapes during the New Year [6]. Z. Li et al. proposed a landscape image feature extraction and retrieval method based on image processing for the management and retrieval of landscape images. This method quantified the color of an image to analyze its color composition and color space patterns. Multi-dimensional color feature vectors were used to match weighted color blocks. Compared to other methods, this method significantly improved the landscape image retrieval [7]. W. Sun proposed a landscape spatial hierarchical planning method for landscape feature extraction. This method calculates planning risks and extracts planning features by analyzing the characteristics and risks of sustainable development in gardens. Under the constraints of landscape spatial hierarchical planning and design requirements, the design conditions of the plant landscape area were calculated. Compared to other methods, this method had a feature extraction accuracy of 98% [8].

After extracting landscape features, to achieve reasonable planning and layout of landscape LID facilities, a suitable layout planning model is also needed. Y. Ke et al. proposed a three-objective mixed-integer linear programming model for the size optimization problem of wind-photovoltaic-hydrogen storage integrated energy systems. This model introduces intuitionistic fuzzy numbers to determine the weights of indicators, aiming to improve the accuracy of decision-making. The experimental results show that the model can achieve a 15% reduction in annual comprehensive cost, a 26% reduction in annual carbon emissions, and an 84% reduction in external power dependence [9]. X. Qi et al. proposed a dynamic virtual inertia control technology based on tracking differentiators to address the issue of inertia reduction in the power grid. The concept of this technology involves deriving the derivative of frequency deviation, which can suppress the adverse effects of noise amplification. Experimental results demonstrate that this control method can effectively ensure the inertia of the power grid [10]. H. Pei et al. proposed a particle swarm optimization-based layout optimization (LO) method for the arrangement of indoor visible light communication lead light sources. This method replaced the traditional circular layout pattern with a polygonal layout model. The polygonal layout was further optimized using the particle swarm optimization algorithm, resulting in an 8.64% improvement in illumination uniformity [11].

In summary, the current research on LO has been quite effective. However, there is relatively little research on landscape LID layout. Most layout studies on landscape LID facilities have not taken into account the uniqueness of the landscape, resulting in poor universality of existing methods. The Revit Building Information Modeling (Revit BIM) system can obtain landscape images through image collection devices and extract their features. The Non-Dominated Sorting Genetic Algorithm III (NSGA-III) performs a global search by mimicking the genetic evolution of organisms and demonstrates strong multi-objective optimization performance. Therefore, to optimize landscape LID facilities' layout, this paper proposes a landscape LID facility LO model based on Revit BIM and NSGA-III. This model innovatively utilizes three descriptors: density, moment of inertia, and geometric moment to extract and describe landscape features. NSGA-III is combined with the Future Land Use Simulation (FLUS) model to achieve reasonable optimization of landscape LID facilities. The contribution of the research lies in: firstly, the study provides an excellent landscape feature extraction method, which helps to rationalize and scientize landscape design and LID facility layout. Secondly, a research method for optimizing the overall site selection and layout of low-impact development facilities has been developed, enriching the field of methodological research. This not only solves the

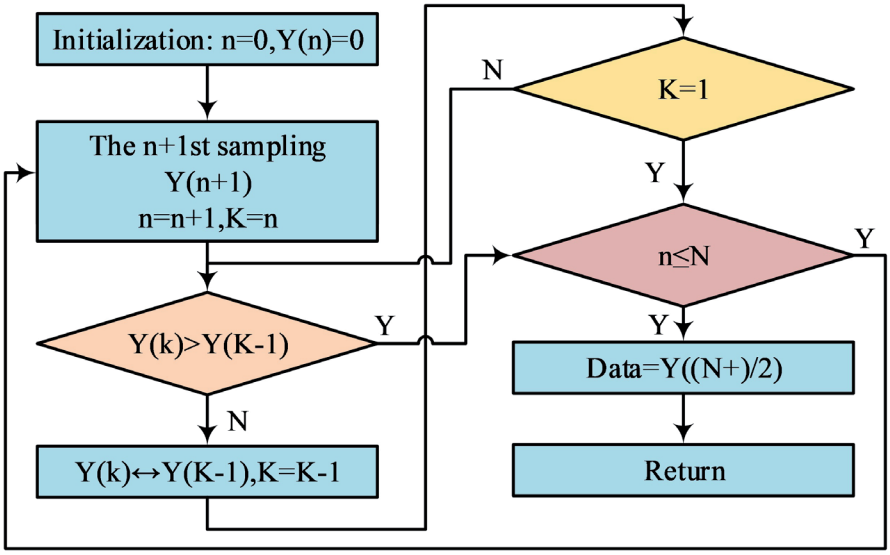

Fig. 1. Process of median filtering.

problem of land shortage in the current sponge city construction process, but also reduces construction costs and difficulties, and maximizes the optimal effect of low-impact development facilities. It has practical significance in providing new thinking, new perspectives, scientific quantitative analysis support, and a decision-making basis for the research of sponge city planning and construction.

The article is divided into four parts. The first part is the research method, which will study the feature extraction of landscape images and the optimization method of LID facility layout. The second part is the experimental results, which will analyze the results of landscape image feature extraction and LID facility layout optimization testing. The third part is the discussion, which will compare and analyze the methods proposed in the study with current methods. The fourth part is the conclusion, which will summarize the research of the entire text.

Methods and Materials

Firstly, the study utilizes the Revit BIM system to extract landscape images and accurately reflect their layout characteristics. This makes landscape design more reasonable and reduces its impact on rainwater discharge in surrounding areas. Then, NSGA-III is used to optimize the landscape layout and achieve the LID layout of landscape facilities.

Landscape Image Extraction Based on Revit BIM

To reduce the difficulty of landscape image extraction and minimize irrelevant information, grayscale processing of the image must first be performed. During grayscale processing, only the main information, such as texture, contour, and position, needs to be retained. The calculation for converting color images to grayscale images is represented by equation (1).

$$Grayscaleimage = Gray0.2989 * R + 0.5870 * G + 0.1140 * B \quad (1)$$

In equation (1), *Grayscaleimage* represents a grayscale image. *Gray* means a pixel value. *R* means a red component. *G* means a green component. *B* means a blue component. The coefficients in the equation are calculated based on the sensitivity of the human eye to different colors. As the human eye has the highest sensitivity to green and relatively low sensitivity to red and blue, the coefficient for green is the highest, while the coefficients for red and blue are smaller. Although grayscale processing can reduce irrelevant information in images, grayscale images contain a large amount of noise, leading to image distortion. Therefore, it is necessary to filter it to obtain clear images. When filtering, to ensure that the complete object contour can be retained after filtering, the median filtering method is chosen as the filtering algorithm. Median filtering is a nonlinear signal processing method and also a statistical sorting filter. It can set the grayscale value of each pixel as the median grayscale value of all pixels within a neighboring window of that point. Median filtering has a good filtering effect on isolated noisy pixels, such as salt and pepper noise and impulse noise. This can maintain the edge characteristics of the image without causing significant blurring [12-14]. Fig. 1 shows the median filtering process.

In Fig. 1, the median filter first uses a two-dimensional sliding template with a certain structure to sort the pixels inside the board according to the size of their pixel values. As a result, a two-dimensional data sequence with monotonic rise or fall is generated. Then, a point value in a digital image or sequence is replaced with each point's median in a neighborhood of that

point. This can make the ambient pixel values close to the truthful values, thus removing isolated noise points [15, 16]. When selecting the filtering window, to ensure the filtering speed, the study chooses a square filtering window. The median filtering output of the square filtering window is represented by equation (2).

$$y_{i,j} = \left| Med\left\{x_i\right\}\right| = Med\left\{x_{i-u}, \cdots, x_i, \cdots, x_{i=u}\right\} \quad (2)$$

In equation (2), $y_{i,j}$ represents the median filtering output. x_i represents a grayscale value. $u=(n-1)/2$. n represents the length of the square filtering window. *Med* represents median filtering. After filtering the grayscale image, image distortion may occur. Therefore, histogram equalization should be performed on the filtered image to improve the grayscale pixel values and ensure the clarity of the image. The probability of generating grayscale pixels during histogram equalization is represented by equation (3).

$$P(i) = m_i / m, \quad i \in 0,1,\cdots L-1 \quad (3)$$

In equation (3), $P(i)$ means pixel generation's probability. m represents the total pixels of the image. L represents the image's grayscale level. Next, the image is balanced using the aggregation and dispersion function, which is represented by equation (4).

$$i = \sum_{j=0}^{i} P(j) = \sum_{j=0}^{i} m_i / m, \quad i \in 0,1,\cdots, L-1 \quad (4)$$

In equation (4), $c(i)$ represents the aggregation normalization function. The histogram of the image can be equalized through the aggregation normalization function. The processed image pixel grayscale value is represented by equation (5).

$$i = c(i) * (L-1) = \sum_{j=0}^{i} m_i / m(L-1), \quad i \in 0,1,\cdots, L-1 \quad (5)$$

In equation (5), i represents the value after grayscale transformation. After processing with the above method, only the main information remains in the collected landscape images, whose feature points can be extracted at this time. To fully extract feature points, it is necessary to ensure the independence between each feature point. Therefore, the study utilizes Principal Component Analysis (PCA) to reduce the data dimensionality. Fig. 2 is a schematic diagram of PCA dimensionality reduction.

In Fig. 2, a set of high-dimensional data is stored in the initial image space. If feature extraction is performed directly on it, the reliability of the extraction results will be poor. Therefore, PCA orthogonal transformation features should be used to convert high-dimensional data in the initial image space into low-dimensional data [17]. The covariance matrix of the initial image space is represented by Equation (6).

$$\sum_x = 1/m \sum_{i=0}^{m} (x_i - \mu)(x_i - \mu)^T \quad (6)$$

In equation (6), $\sum_x$ represents the covariance matrix. μ represents all sample sets' mean vectors in the primitive image space. The eigenvectors and eigenvalues's relationship in the covariance matrix is represented by equation (7).

$$U(\lambda I - \sum_x) = 0 \quad (7)$$

In equation (7), U represents the feature vector. λ represents the characteristic value. I represents the identity matrix. At this point, the PCA orthogonal transformation is represented by equation (8).

$$Y = W^T X \quad (8)$$

In equation (8), W represents the PCA transformation matrix. X represents data within the image space. By substituting the feature values in the image into equation (8), all feature points can be identified independently. After completing the dimensionality reduction of image data, it is necessary to describe the regional shape features of the landscape. To ensure the accuracy of describing shape features, the study utilizes density sets, moment of inertia, and geometric moments to extract shape features. The perimeter of the landscape area will vary with the changes in the target area. The shape areas with dense landscape features are circular. Therefore, the density set is represented by equation (9).

$$C = \frac{P^2}{4\pi A} \quad (9)$$

In equation (9), C represents the density set. P represents the perimeter of the landscape area. A represents the area of the landscape area. In addition, since the center of gravity of the target area is a comprehensive description of the shape feature area, it is necessary to calculate the rotation management. The normalized moment of inertia is represented by equation (10).

$$NMI = \sqrt{J(c_x, c_y)} \Big/ p = \sqrt{\sum_{x=1}^{M}\sum_{y=1}^{N}\left((y-c_y)^2 + (x-c_x)^2 f(x,y)\right)} \Big/ \sum_{x=1}^{M}\sum_{y=1}^{N} f(x,y) \quad (10)$$

In equation (10), NMI represents the normalized moment of inertia. $J(c_x,c_y)$ represents the moment of

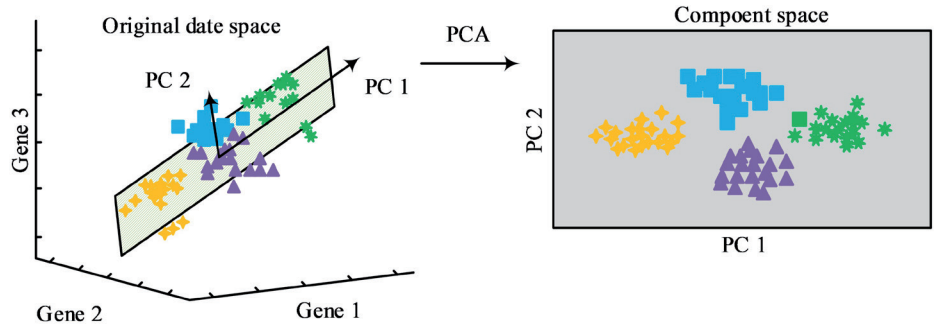

Fig. 2. Schematic diagram of the dimension reduction in PCA.

inertia around the mass center (c_x,c_y). p represents the quality of landscape images, which is the sum of the landscape's all grayscale values. $f(x,y)$ represents a grayscale image. M and N represent the quantity of grayscale images and centroids, respectively. To ensure the accuracy of shape features, it is also necessary to calculate geometric moments. It is assumed that there exists a piecewise continuous probability density distribution function and a two-dimensional continuous random function. By using a piecewise continuous probability density distribution function, it is possible to confirm each order's moment sequence of this function, which is a unique sequence [18-20]. At this point, the geometric moment, also known as the center moment, is represented by equation (11).

$$\begin{cases} m_{pq} = \int_{-\infty}^{+\infty}\int_{-\infty}^{+\infty} y^q x^p f(x,y)\,dxdy \\ u_{pq} = \int_{-\infty}^{+\infty}\int_{-\infty}^{+\infty} (y-\overline{y})^q (x-\overline{x})^p f(x,y)\,dxdy \end{cases} \tag{11}$$

In equation (11), m_{pq} represents geometric moments. p and q mean matrix orders. $g(x,y)$ represents a piecewise continuous probability density distribution function. u_{pq} represents the center moment. $(\overline{x},\overline{y})$ represents the image centroid. After extracting the pixels of different feature descriptors through the above method, pixel fusion processing can be performed on them. Based on this, the differential features of the landscape can be extracted. The process of extracting the differences in landscape features is as follows. Firstly, the image is subjected to grayscale processing and filtering, and histogram equalization is performed. Then, PCA technology is used to orthogonally transform landscape features to obtain independent features. Then, the density set, moment of inertia, and geometric moments of the landscape image are calculated. These three are fused to obtain the shape features of the landscape. Then, the shape features are fused with the independent feature points obtained after PCA dimensionality reduction to ultimately achieve feature extraction of the landscape.

Landscape LID Facility Layout Optimization Based on NSGA-III

When designing and constructing landscapes, it is inevitable that they will have an impact on urban rainwater discharge. Therefore, to ensure the runoff control and pollutant reduction effect of urban rainwater, a landscape LID facility LO model based on NSGA-III is constructed on the basis of Revit BIM landscape image extraction. This model is based on the System for Urban Stormwater Treatment and Analysis Integration Model (SUSTAIN) from the United States. The study improves the efficiency and effectiveness of landscape facility LID layout by optimizing its modules. SUSTAIN can control runoff, peak runoff, and reduce pollutants by setting up Low Impact Development/Best Management Plan (LID/BMP) facilities to infiltrate and retain rainfall. SUSTAIN can also conduct cost management and optimization analysis, evaluate the costs and benefits of different combinations of LID/BMP facilities, and layout planning schemes [21-23]. The unit area outflow of a city is represented by equation (12).

$$Q = B\frac{1.49}{z}\left(d-d_p\right)^{5/3} s^{1/2} \tag{12}$$

In equation (12), Q refers to the unit area outflow when the surface water depth exceeds the depression depth. w refers to the width of a sub-watershed. *man* refers to Manning's coefficient. d and d_p correspond to water depth and depression depth. s refers to the depression slope. The SUSTAIN design adopts a modular structure, consisting of seven modules: framework management, BMP layout, land simulation, BMP simulation, transmission simulation, optimization, and post-processing program. Framework management is the command center of the model, calling other model blocks, managing data transformation, and so on. BMP layout is mainly responsible for the site selection of BMP. The land simulation module has two methods: internal and external simulation. Internal simulation uses the algorithm in SWMM5 to calculate hydrological and water quality process lines. External simulation can utilize the simulation results of other models as input data for SUSTAIN without the need for recalculation in

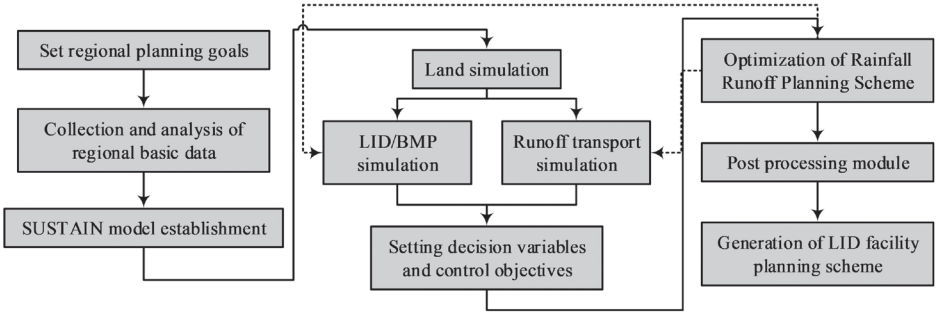

Fig. 3. The LID facility layout planning system.

SUSTAIN. BMP simulation will enable the simulation calculation, degradation, and transport processes of runoff and pollutants. This module also includes a cost estimation component that can calculate the cost of BMP measures based on local raw material prices [24-26]. The dynamic equation of non-polluting sediment in pipelines in transmission simulation is represented by equation (13).

$$C_t = C_0 e^{-kt} \tag{13}$$

In equation (13), C_t represents the concentration of non-polluting sediment at time t. C_0 represents the initial concentration of non-polluting sediment. k represents the reaction rate constant. The optimization module mainly achieves LID/Best Management Plan (BMP) facility optimization through decentralized search algorithms and NSGA-II. The congestion distance of NSGA-II is based on the same non-dominated level, making it difficult to achieve multi-objective optimization. NSGA-III selects congestion distance based on reference points, thus obtaining the optimal solution set widely distributed on the Pareto optimal frontier and achieving multi-objective optimization [27]. The quantity of reference points is represented by equation (14).

$$\begin{cases} N_{refcount} = \left(\dfrac{T+H-1}{H} \right), & target \le 5 \\ N_{refcount} = \left(\dfrac{T+H_{in}-1}{H_{in}} \right) + \left(\dfrac{T+H_{out}-1}{H_{out}} \right) & target > 5 \end{cases} \tag{14}$$

In equation (14), $N_{refcount}$ represents the quantity of reference points. T represents the target quantity. H represents the quantity of partitions on a single target axis. H_{in} represents the quantity of partitions on the target axis of the inner reference point hyperplane. N_{out} represents the quantity of partitions on the hyperplane target axis of the outer reference point. The use of land can also have an impact on urban rainwater discharge. Therefore, the study additionally introduces the FLUS model to further optimize the layout of landscape LID facilities. Firstly, the correspondence between landscape land use types, rainwater runoff control, pollutant reduction effects, and other factors is determined through artificial neural networks to achieve a low-impact layout of landscape facilities, represented by equation (15).

$$\begin{aligned} sp(q,r,t) &= \sum_j \omega_{j,r} \times sigmoid\left(net_j(q,t) \right) \\ &= \sum_j \omega_{j,r} \times \left[1 + e^{net_j(q,t)} \right]^{-1} \end{aligned} \tag{15}$$

In equation (15), $sp(q, r, t)$ represents the low impact probability of the rth landscape at grid q and time t. $\omega_{j,r}$ represents the hidden and output layers' weight value. $n_j(q, t)$ represents the signal received by the jth hidden layer grid q at time t. The optimization objective and constraint of landscape facility LID layout are represented by equation (16).

$$\begin{cases} minimize \sum_{i=1}^{n} \cos t\left(BMP_i \right) \\ Q_j \le Q_{\max,j} or L_k \le L_{\max,k} \end{cases} \tag{16}$$

In equation (16), BMP_i represents the LID/BPM facility with ID i. Q_j represents the total simulated water volume at point j. $Q_{max,j}$ represents the maximum water quantity limit at point j. L_k represents the total simulated water quality. $L_{max,k}$ represents the maximum limit of water quality. Through the above methods, the LO of landscape facilities can be achieved. However, to ensure the cost-effectiveness of LO, it is also necessary to establish a reasonable layout planning system. Fig. 3 shows the LID facility layout planning system.

In Fig. 3, the LID facility planning system based on cost-benefit optimization management includes setting regional control objectives, data collection, and analysis processing, model establishment, planning scheme optimization, and result analysis expression. It is worth noting that when collecting and analyzing data, detailed information on the local topography, existing drainage plans, and climate should be gathered to support subsequent LID layout planning [28, 29]. Table 1 shows the input parameters and sources of SUSTAIN.

In Table 1, the input parameters of SUSTAIN include land use type, land use attributes, soil type,

Table 1. Input parameters of the SUSTAIN model.

Data name	Data description	Data sources
Land use type map	Vector data	Field exploration report information
Land use property table	Attribute data table	Basic data integration and extraction
Digital elevation map	Raster data	Field exploration report information
Soil type map	Vector data	Exploration report information extraction and generation
Soil type properties table	Attribute data table	Exploration report information extraction and generation
Water permeability distribution map	Raster data	The author integrated the analysis that was obtained
Classification map of catchment area	Vector data	The author integrated the analysis that was obtained
Rainfall data	Text file	State meteorological administration
Meteorological data	Text file	State meteorological administration
Hydrohydrohydraulic parameters	The Manning coefficient in the impervious zone	Summary and induction of literature
	Depression storage capacity in the impervious area	Summary and induction of literature
The LID facility characteristic parameters	Length, width, matrix, and other characteristics	Summary of the literature and local data
The LID facility cost database	Database	Summary of the literature and local data

permeability, rainfall data, meteorological data, LID facility characteristics, etc. Since SUSTAIN can only recognize English units, it is necessary to convert metric units to English units before inputting parameters. In addition, in SUSTAIN's runoff calculation, a suitable infiltration model for the catchment area should be constructed. After considering parameters such as the width of the sub-catchment area, the Horton formula is empirically chosen for the infiltration rate, as represented by Equation (17).

$$f(t) = f_c + (f_0 - f_c) * e^{-at} \tag{17}$$

In equation (17), $f(t)$ means the infiltration rate. f_c represents the stable infiltration rate. f_0 represents the initial infiltration rate. a represents the infiltration attenuation constant. In addition, the design parameters of LID facilities will greatly affect the effectiveness of rainwater discharge. Therefore, referring to the "Sponge City Construction Technical Guide" and related literature, reasonable values should be assigned to the design parameters of bioretention facilities and tree-planting ditches. Table 2 shows the parameters of biological retention facilities.

In Table 2, the drainage area of the bioretention facility is 0.05 ac. The field water holding capacity of the soil is 0.25. The saturated soil infiltration rate and maximum infiltration rate are 1 in/h and 4 in/h, respectively. The attenuation coefficient and drying days are 4 and 7, respectively. Table 3 shows the design parameters for grass-planting ditches.

In Table 3, the length, width, drainage area, saturated soil infiltration rate, maximum infiltration rate, attenuation coefficient, and drying days of grass-planting ditches are consistent with those of biological retention facilities. The soil depth is 0.98 feet. The field water holding capacity of the soil is 0.3. The uncertainty of parameters is high. As the model runs, uncertainty gradually accumulates. Therefore, to ensure the reliability of the simulation results, these parameters should be calibrated and verified. The LID facility can ensure the discharge of rainwater. However, to maximize the effectiveness of rainwater discharge management, it is necessary to have a reasonable layout and connection of various LID facilities. Fig. 4 shows the LID facility connection method.

In Fig. 4, when rainfall occurs, after the rainwater falls to the roof and ground, it will first infiltrate through the green roof and permeable pavement to the biological retention pool and grass ditch. At this time, if the rainfall is too large, the biological retention tank cannot fully absorb the seepage rainwater. The excess rainwater beyond the biological retention tank's capacity will continue to infiltrate into the grass-planting ditch. Excess rainwater that surpasses the capacity of biological retention tanks and grass ditches will be directed into the rainwater pipe network, ensuring the removal of surplus water and preventing urban waterlogging.

Table 2. Biological retention facility parameters.

LID installation	Biological retention facilities	
Configuration parameter	Length	16 ft
	Width	16 ft
	Drainage area	0.05 ac
Matrix characteristics	Depth of soil	1.64 ft
	Soil porosity	0.5
	Soil and field water holding capacity	0.25
	Soil withered point	0.15
	Saturated soil infiltration rate	1 in/h
Osmotic coefficient	Maximum lower percolation rate	4 in/h
	Attenuation coefficient	4
	Drought days	7
Cost parameters	Unit construction cost	47.79 CNY/ft^2

Results and Discussion

The study tested the image extraction and LO performance to validate the proposed landscape LID facility LO method.

Analysis of Landscape Image Extraction Effect

When verifying the effectiveness of landscape image extraction, the study was tested on the Matlab2010 platform. Comparisons were made with Multi-threshold Optimization (MTO) and Linear Backprojection-Gray Level Co-occurrence Matrix (LBP-GLCM). The dataset used is a self-made dataset, consisting of 1324 landscape images, with 662 images in each of the experimental and training sets. The CPU used is Intel Core i5 12600KF. The GPU is NVIDIA RTX40 4060 Ti. The memory is 32GB and the operating system is Windows 10. Fig. 5 shows the accuracy of feature point classification and Peak Signal-to-Noise Ratio (PSNR) for each algorithm.

In Fig. 5 (a), the feature point classification accuracy of MTO and LBP-GLCM was the highest at 91.1% and 88.8%, respectively, and the lowest at 86.4% and 85.3%, with an average accuracy of 88.9% and 87.7%, respectively. The accuracy of Revit BIM was the lowest at 86.6%, the highest at 97.4%, and the average accuracy was 91.9%. The accuracy of feature point recognition in Revit BIM was much higher than in other algorithms. In Fig. 5 (b), the maximum PSNR of MTO and LBP-GLCM was 0.053 and 0.050, respectively, and the lowest

Table 3. Design parameters of grass ditch.

LID installation	Grass-planting ditch	
Configuration parameter	Length	16 ft
	Width	16 ft
	Drainage area	0.05 ac
Matrix characteristics	Depth of soil	0.98 ft
	Soil porosity	0.5
	Soil and field water holding capacity	0.3
	Soil withered point	0.15
	Saturated soil infiltration rate	1 in/h
Osmotic coefficient	Maximum lower percolation rate	4 in/h
	Attenuation coefficient	4
	Drought days	7
Cost parameters	Unit construction cost	23.90 CNY/ft^2

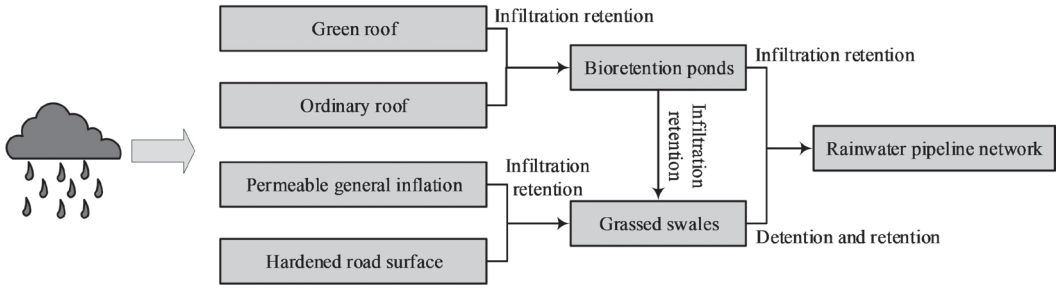

Fig. 4. Connection mode of the LID facilities.

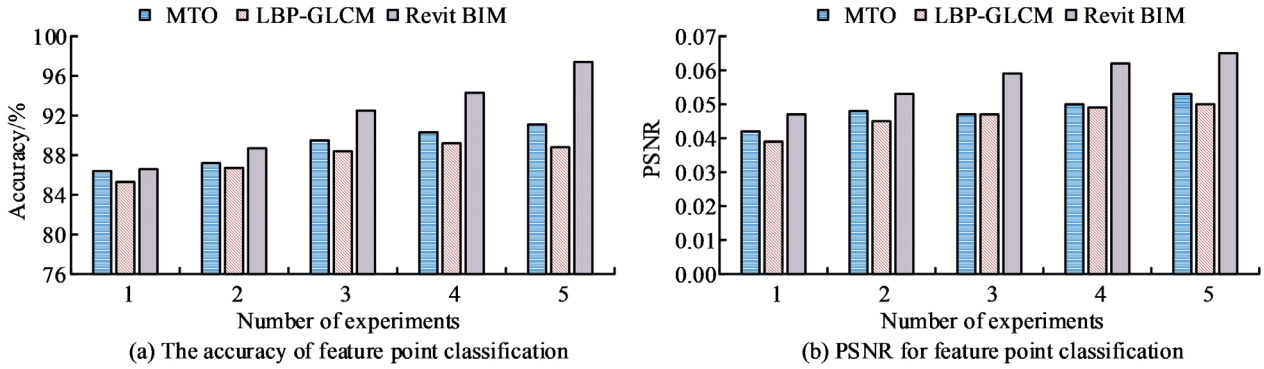

Fig. 5. Feature point classification accuracy and peak signal-to-noise ratio.

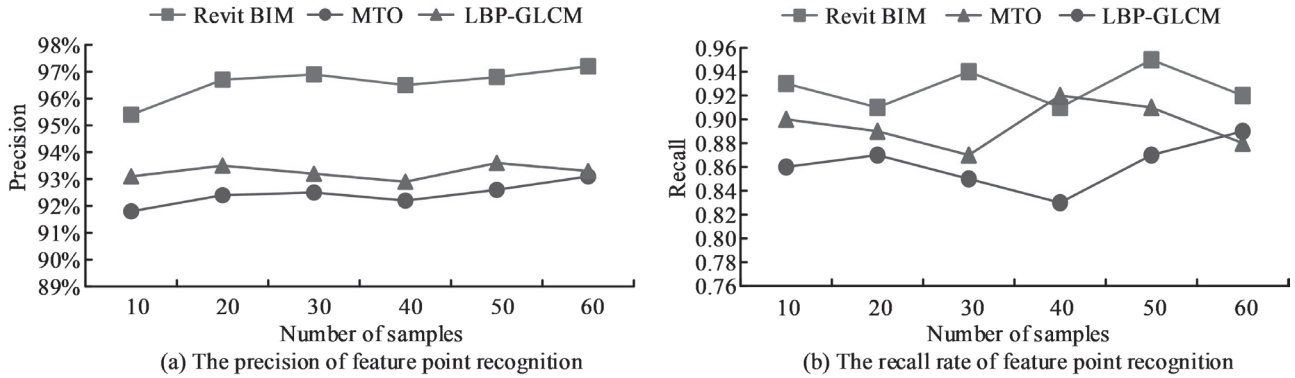

Fig. 6. Characteristic point extraction precision and recall rate of each algorithm.

at 0.042 and 0.039, respectively, with an average PSNR at 0.048 and 0.046. The minimum PSNR of Revit BIM was 0.047, with an average PSNR at 0.057, which was higher than other algorithms. The proposed landscape image feature extraction model based on Revit BIM accurately extracted feature points while reducing image noise. Fig. 6 shows the precision and recall of feature point extraction for each algorithm.

In Fig. 6 (a), the feature point classification precision of MTO and LBP-GLCM was the highest at 93.1% and 93.6%, respectively, and the lowest at 91.8% and 92.9%, respectively. The recognition precision of Revit BIM was highest at 97.2% and lowest at 95.4%, which was higher than other algorithms. In Fig. 6 (b), the highest feature point classification recall for MTO and LBP-GLCM was 0.92 and 0.89, respectively, and the highest at 0.87 and 0.83, respectively. The recall of Revit BIM was highest at 0.95 and lowest at 0.91. Revit BIM accurately recognized image features. Fig. 7 shows the feature point extraction time for each algorithm.

In Fig. 7, the feature point extraction time of each algorithm increased with the increasing image size. When the image size was 2*2, the feature point extraction time for both MTO and Revit BIM was 15s, while the feature extraction time for LBP-GLCM was 22s. When the image size increased to 16*16, the feature point extraction time for MTO and LBP-GLCM was 23s and 42s, respectively, while the feature point extraction time for Revit BIM was only 21s. Compared to MTO and LBP-GLCM, the feature point extraction speed of

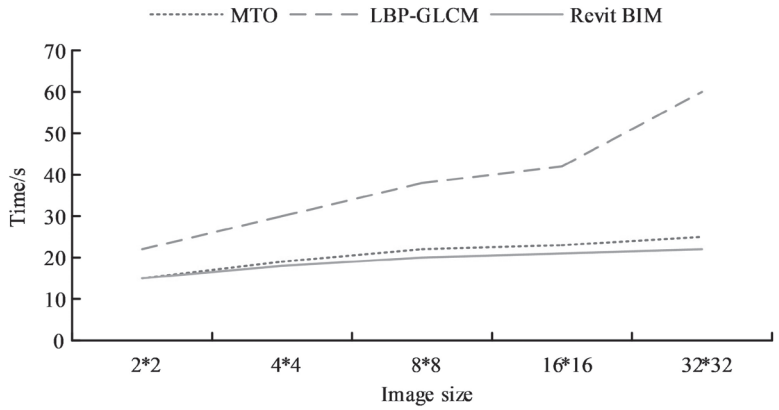

Fig. 7. Characteristic point extraction time for each algorithm.

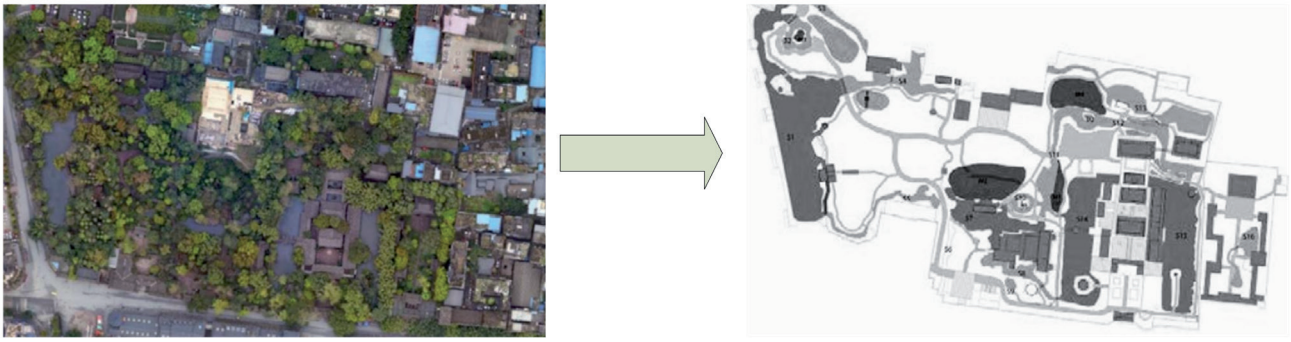

Fig. 8. Feature extraction results of Revit BIM.

Revit BIM was faster. Fig. 8 shows the feature extraction results of Revit BIM using a certain garden landscape as an example.

In Fig. 8, the proposed landscape feature extraction method based on Revit BIM effectively removed obstructions such as trees and grasslands. This method achieved the extraction of landscape features, accurately reflecting the overall layout and element planning of the landscape.

Analysis of Optimization Results of Landscape LID Facility Layout

The study used a certain garden landscape as an example to validate the proposed landscape LID facility LO model. Fig. 9 shows the LID facility site selection results for the landscape.

In Fig. 9, the area of all site selection results accounted for approximately 18% of the total landscape area. Specifically, the site selection results for biological retention ponds, grass-planting ditches, and permeable paving were basically consistent. However, in terms of spatial requirements, there was no building buffer distance or river buffer distance for grass-planting ditches. Therefore, the overall suitable construction land was more than that of biological retention ponds. The main building of this landscape is an ancient building, which has certain protection requirements. Therefore, it is not possible to renovate the main building to install a biological roof. Fig. 10 shows the LID facility site selection planning layout for the landscape.

In Fig. 10, rainwater will first enter the green roof and permeable pavement, so that the rainwater in the catchment area can fully infiltrate underground and be retained in the biological retention pool and grass ditch. The optimized LID facility layout added biological retention tanks, permeable paving, and grass-planting ditches compared to the original rainwater drainage facilities. The location of the generalized rainwater well was slightly changed compared with its original location so that the rainwater could be discharged in time in case of a rainstorm. Fig. 11 shows the optimized distribution area and cost-benefit curve of LID facilities.

In Fig. 11 (a), sub-catchment area 7 had the largest area. Therefore, the area of the biological retention pool, grass-planting ditch, and permeable pavement in this area was the largest, with 900m^2, 960m^2, and 600m^2, respectively. Through this LID facility layout method, the rainwater runoff in the area was effectively reduced. In Fig. 11 (b), the annual rainfall in the area where the landscape was located decreased significantly compared to previous years. Therefore, when selecting the optimization plan for LID facilities, the study selected a LID facility layout and construction plan that balanced

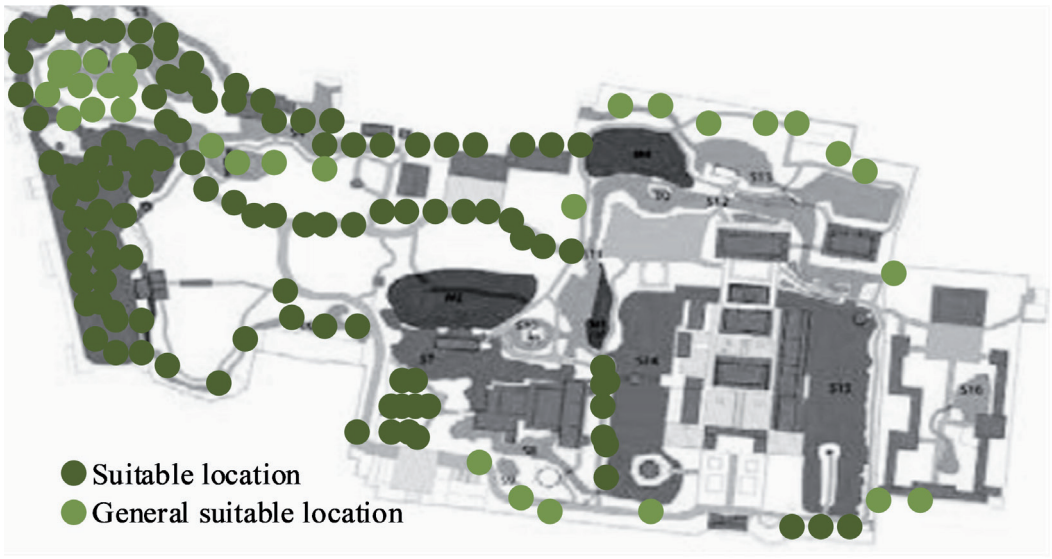

Fig. 9. LID facility site selection results for the landscape.

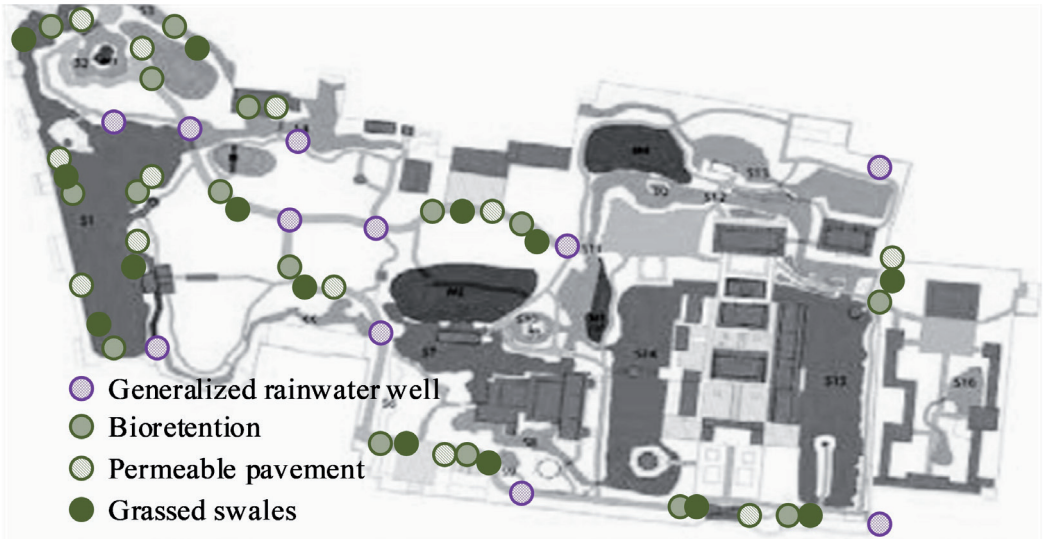

Fig. 10. Location planning and layout of LID facilities.

construction costs and rainwater treatment benefits. The construction cost and annual runoff reduction rate of this plan were 397500 CNY and 87.0%, respectively. By implementing the selected LID facility optimization layout plan, the rainwater runoff in the landscape area could be effectively reduced. Fig. 12 shows the cost and reduction rate of each LID facility's LO plan.

In Fig. 12 (a), the most suitable implementation area for biological retention tanks, grass-planting ditches, and permeable paving was 5651m^2, 10424m^2, and 3953m^2, respectively. The costs were 156700 CNY, 124900 CNY, and 115900 CNY, respectively. In Fig. 12 (b), the available site area for biological retention tanks, grass-planting ditches, and permeable paving was 13257m^2, 27123m^2, and 9764m^2, respectively. The facility area was 4662m^2, 7231m^2, and 3154m^2, respectively. The optimization reduction rates were 78%, 59%, and 70%, respectively. After optimization, all LID facilities could achieve a reduction rate of over 55% in rainwater runoff. Fig. 13 shows the cost and area ratio of each LID facility.

In Fig. 13, the cost and area proportions of permeable pavement were 29.16% and 20.96%, respectively. The cost and area proportion of grass-planting ditches were 31.42% and 48.06%, respectively. The cost and area proportion of biological retention tanks were 39.42% and 30.98%, respectively. Therefore, in the optimization plan of LID facilities in the study area, the area of biological retention tanks accounted for the largest proportion, while the cost of grass-planting ditches accounted for the largest proportion.

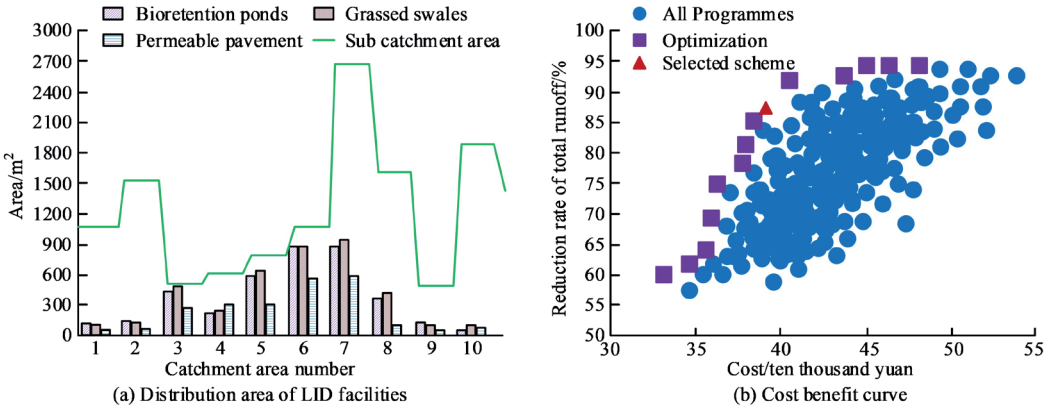

(a) Distribution area of LID facilities (b) Cost benefit curve

Fig. 11. Distribution area and cost-benefit curve of optimized LID facilities.

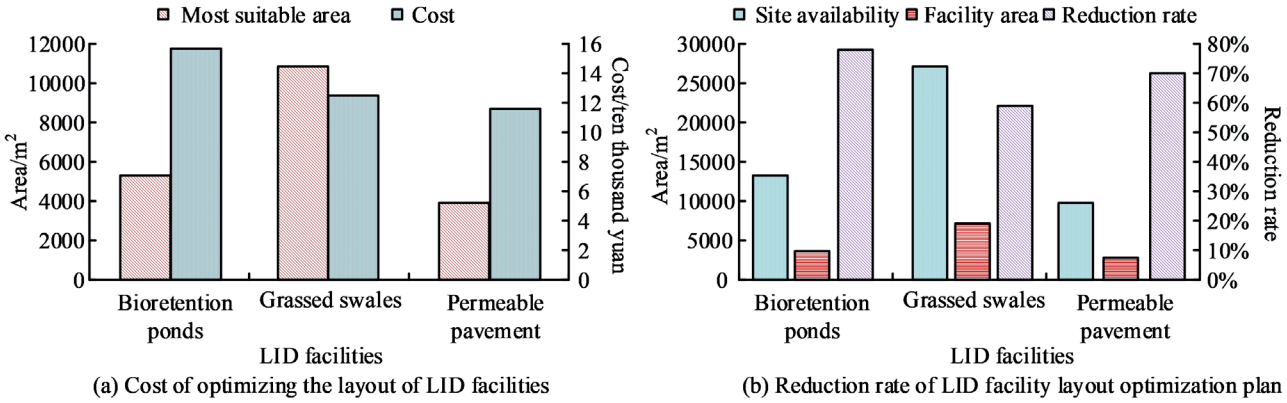

(a) Cost of optimizing the layout of LID facilities (b) Reduction rate of LID facility layout optimization plan

Fig. 12. Cost and reduction rate of each LID facility layout optimization scheme.

Discussion

The planning and construction of landscapes often have a certain impact on rainwater discharge in surrounding areas. Therefore, LID facilities should be reasonably laid out during landscape construction to ensure the normal discharge of rainwater. However, each landscape area has different characteristics. When planning the layout of LID facilities in scenic areas, the landscape area's features should first be extracted. Current landscape feature extraction methods, however, suffer from poor accuracy, low efficiency, and low PSNR in feature point classification. To address these issues, a landscape feature extraction method based on Revit BIM is proposed. This method achieves an average accuracy of 91.9%, which is higher than that of MTO and LBP-GLCM. This is because Revit BIM not only performs grayscale processing on landscape images but also performs median filtering denoising and histogram equalization to improve image pixels. In addition, this method also uses PCA technology to perform orthogonal transformations on features to obtain new feature patterns, making the feature points uncorrelated. The shape features are described using density sets, moment of inertia, and geometric moments to ensure their accuracy. For the LO problem of LID facilities, the research adopts improved SUSTAIN for optimization. This model can reduce the annual total runoff by 87.0%, greatly ensuring the effectiveness of rainwater discharge. This is because the improved SUSTAIN utilizes NSGA-III and FLUS to optimize the layout of LID facilities. Compared to SUSTAIN's original NSGA-II, NSGA-III selects congestion distance based on reference points. Therefore, NSGA-III can obtain the optimal solution set widely distributed on the Pareto optimal frontier, thereby achieving multi-objective optimization. The FLUS model can accurately reflect the land use situation and provide strong support for the layout of LID facilities.

Conclusions

To reduce the impact of landscape construction on rainwater discharge in surrounding areas and reduce construction costs, a landscape LID facility LO method based on Revit BIM and NSGA-III is proposed. This method utilizes Revit BIM to extract landscape features and optimizes the layout of LID facilities using an improved SUSTAIN based on NSGA-III. The highest accuracy of Revit BIM was 97.4%, with an average accuracy of 91.9% and an average PSNR of 0.057, all

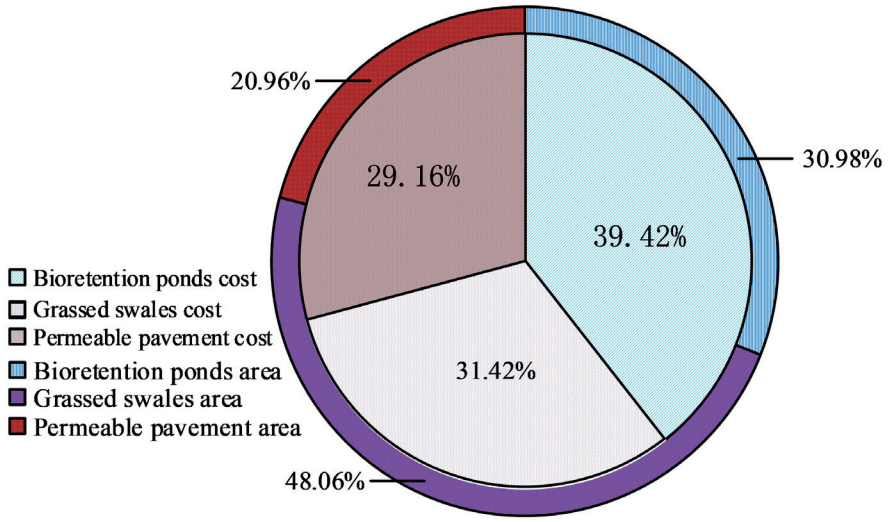

Fig. 13. Cost and area ratio of each LID facility.

higher than other algorithms. In addition, when the image size was 16*16, the feature point extraction time of Revit BIM was only 21s, which was less than other algorithms. In terms of LID facility LO, the LID facility optimized by the improved SUSTAIN had a construction cost reduction rate of 397500 CNY and an annual runoff reduction rate of 87.0%, respectively. The optimized reduction rates for biological retention ponds, grass-planting ditches, and permeable paving were 78%, 59%, and 70%, respectively. The proposed landscape LID facility LO method based on Revit BIM and NSGA-III could optimize landscape LID facilities, greatly reduce rainwater runoff, and ensure timely drainage of rainwater. However, when setting the relevant parameters for each sub-catchment area, the study only refers to relevant literature and does not conduct field measurements, resulting in certain differences between experimental results and actual results. Therefore, in the future, the model parameters will be modified to ensure its actual optimization effect.

Acknowledgments

This research did not receive any specific grant from funding agencies in the public, commercial, or not-for-profit sectors.

Conflict of Interest

The authors declare no conflict of interest.

References

1. HAN C.L., XIONG X.Z., CHEN Y., LIU X.X. A runoff pollution control technology in sponge service area based on concept of low-impact development. Transport Research, **9** (2), 42, **2023.**
2. JOB C. A review of low-impact development factors affecting managed aquifer recharge. Ground water. Journal of Ground Water, **60** (5), 619, **2022.**
3. HOU J.W., SUN S.Q., WANG Y.J., WANG J.R., YANG C. Comparison of runoff from low-impact development measures in arid and humid cities. Proceedings of the Institution of Civil Engineers. Water Management, **175** (3), 135, **2022.**
4. ZHOU Y., SHE D., WANG Y., XIA J., ZHANG Y. Evaluating the impact of low impact development practices on the urban flooding over a humid region of China. Journal of the American Water Resources Association, **58** (6) 1264, **2022.**
5. SHEN H., XU Z. Monitoring and evaluating rainfall–runoff control effects of a low impact development system in future science park of Beijing. Journal of the American Water Resources Association, **57** (4), 638, **2021.**
6. ZHANG Q., ZHANG J., LU S., LIU Y., LIU L., WANG Y., CAO M.Y. Multi-resolution feature extraction and fusion for traditional village landscape analysis in remote sensing imagery. Traitement du Signal, **40** (3), 1259, **2023.**
7. LI Z., HAN X., WANG L., ZHU T., YUAN F. Feature extraction and image retrieval of landscape images based on image processing. Traitement du Signal, **37** (6), 1009, **2020.**
8. SUN W. Hierarchical planning method of garden plant in landscape space under the concept of sustainable development. International Journal of Environmental Technology and Management, **24** (3), 200, **2021.**
9. KE Y., TANG H., LIU M., MENG Q., XIA Y. Optimal sizing for wind-photovoltaic-hydrogen storage integrated energy system under intuitionistic fuzzy environment. International Journal of Hydrogen Energy, **48** (88), 34193, **2023.**
10. QI X., MADONSKI R., HUANG C., KE Y. Tracking-differentiator-based dynamic virtual inertial control of offshore wind power plant for frequency regulation. International Journal of Electrical Power & Energy Systems, **141,** 108150, **2022.**
11. PEI H., JING L., TONG Z., MA M., CUI X. Layout and optimization of LED light source for indoor visible light communication. Microwave and Optical Technology

Letters, **65** (2), 710, **2023.**
12. ZHAI Q., LI Y., ZHANG Z., LI Y., WANG S. Adaptive feature extraction and fine-grained modulation recognition of multi-function radar under small sample conditions. IET Radar, Sonar & Navigation, **16** (9), 1460, **2022.**
13. NIEPCERON B., GRASSIA F., MOH A.N.S. Brain tumor detection using selective search and pulse-coupled neural network feature extraction. Computing and Informatics, **41** (1), 253, **2022.**
14. XIAO Y. Study on microstructure damage characteristics of asphalt mixture based on multivariate feature extraction. International Journal of Microstructure and Materials Properties, **16** (2), 206, **2022.**
15. RAJESHWARI M.R., KAVITHA K.S. Enhanced tolerance-based intuitionistic fuzzy rough set theory feature selection and ResNet-18 feature extraction model for arrhythmia classification. Multiagent and Grid Systems, **18** (3), 241, **2022.**
16. BOUZIANE A., KHARROUBI J., ZARGHILI A. Towards an objective comparison of feature extraction techniques for automatic speaker recognition systems. Bulletin of Electrical Engineering and Informatics, **10** (1), 374, **2021.**
17. DORNELAS R.S., LIMA D.A. Correlation Filters in Machine Learning Algorithms to Select Demographic and Individual Features for Autism Spectrum Disorder Diagnosis. Journal of Data Science and Intelligent Systems, **3** (1), 7, **2023.**
18. MUHAMMED S., ELEBI E. CAMNet: DeepGait Feature Extraction via Maximum Activated Channel Localization. Intelligent Automation & Soft Computing, **28** (2), 397, **2021.**
19. BAYKARA M., ABDULRAHMAN A. Seizure detection based on adaptive feature extraction by applying extreme learning machines. Traitement du Signal, **38** (2), 331, **2021.**
20. ELMANNAI H.E., NACEUR M.S., LOGHMARI M.A., ALGARNI A. A new feature extraction approach based on non-linear source separation. International Journal of Electrical & Computer Engineering, **11** (5), 4082, **2021.**
21. LI J., LI Y., WANG Y. Fuzzy inference NSGA-III algorithm-based multi-objective optimization for switched reluctance generator. IEEE Transactions on Energy Conversion, **36** (4), 3578, **2021.**
22. ZHENG Y., ZHANG L., PAN Y., HE Z. Multi-objective structural optimization of a wind turbine tower. Journal of Shanghai Jiaotong University, **25** (4), 538, **2020.**
23. ZKAN R., GEN M.S. Multi-objective structural optimization of a wind turbine blade using NSGA-II algorithm and FSI. Aircraft Engineering and Aerospace Technology, **93** (6), 1029, **2021.**
24. JAFARI H., NAZIF S., RAJAEE T. A multi-objective optimization method based on NSGA-III for water quality sensor placement with the aim of reducing potential contamination of important nodes. Water Supply, **22** (1), 928, **2022.**
25. SUN X., XU N., YAO M. Sequential subspace optimization design of a dual three-phase permanent magnet synchronous hub motor based on NSGA-III. IEEE Transactions on Transportation Electrification, **9** (1), 622, **2023.**
26. YANG Y., ZHANG J., SUN W., PU Y. Research on NSGA-III in location-routing-inventory problem of pharmaceutical logistics intermodal network. Journal of Intelligent & Fuzzy Systems, **41** (1), 699, **2021.**
27. TRIVEDI M., SHARMA K. Construction time–cost–resources–quality trade-off optimization using NSGA-III. Asian Journal of Civil Engineering, **24** (8), 3543, **2023.**
28. AMORIM E.A., ROCHA C. Optimization of wind-thermal economic-emission dispatch problem using NSGA-III. IEEE Latin America Transactions, **18** (9), 1555, **2020.**
29. TRNG N.H., DAO D.N. New hybrid approach HNSGA-III&SPEA/R: application to optimization of powertrain mount system stiffness parameters. Journal of Low Frequency Noise, Vibration and Active Control, **40** (4), 1976, **2021.**